Identification and characterization of a murine model of BCR-ABL1$^+$ acute B-lymphoblastic leukemia with central nervous system metastasis

XIAOZHUO YU[1,2], HUA ZHANG[1,2], MENG YUAN[1,2], PING ZHANG[1,2], YANG WANG[1,2], MINGZHE ZHENG[1,2], ZHUANGWEI LV[1,2], WOODVINE OTIENO ODHIAMBO[1,2], CANYU LI[1], CHENGCHENG LIU[1,2], YUNFENG MA[1,2] and YANHONG JI[1,2]

[1]Department of Pathogenic Biology and Immunology, School of Basic Medical Sciences, Xi'an Jiaotong University Health Science Centre; [2]Key Laboratory of Environment and Genes Related to Diseases (Xi'an Jiaotong University), Ministry of Education of China, Xi'an, Shaanxi 710061, P.R. China

Received November 8, 2018; Accepted May 21, 2019

DOI: 10.3892/or.2019.7184

Abstract. Breakpoint cluster region (BCR)-Abelson murine leukemia (ABL)1$^+$ acute B-lymphoblastic leukemia (B-ALL) is a disease associated with a dismal prognosis and a high incidence of central nervous system (CNS) metastasis. However, BCR-ABL1$^+$ B-ALL with CNS infiltration has not been previously characterized, at least to the best of our knowledge. In the present study, a murine model of BCR-ABL1$^+$ B-ALL with CNS metastasis was established using retroviral transduction. The vast majority of BCR-ABL1$^+$ leukemic cells were found to be immature B cells with a variable proportion of pro-B and pre-B populations. The present results indicated that the BCR-ABL1$^+$ B-leukemic cells expressed high levels integrin subunit alpha 6 (Itga6) and L-selectin adhesion molecules, and have an intrinsic ability to disseminate and accumulate in CNS tissues, predominantly in meninges. On the whole, these results provide an approach for addressing the mechanisms of BCR-ABL1$^+$ B-ALL with CNS metastasis and may guide the development of novel therapeutic strategies.

Correspondence to: Dr Yanhong Ji, Department of Pathogenic Biology and Immunology, School of Basic Medical Sciences, Xi'an Jiaotong University Health Science Centre, 76 Yanta West Road, Xi'an, Shaanxi 710061, P.R. China
E-mail: jiyanhong@xjtu.edu.cn

Abbreviations: BCR-ABL1$^+$ B-ALL, Breakpoint cluster region-Abelson murine leukemia acute B-lymphoblastic leukemia; CNS, central nervous system; TKIs, tyrosine kinase inhibitors; SCID, severe combined immunodeficiency; CML, chronic myeloid leukemia; MIG-p210 vector, MSCV-BCR-ABL1-IRES-GFP; MIG vector, MSCV-GFP; SPF, specific pathogen-free; H&E, hematoxylin and eosin; PB, peripheral blood; SP, spleen; LN, lymph node; BM, bone marrow; ST, subcutaneous tumor

Key words: BCR-ABL1$^+$ B-ALL, CNS metastasis, immature B cell, intravascular staining, retroviral transduction

Introduction

Breakpoint cluster region (BCR)-Abelson murine leukemia (ABL)1$^+$ acute B-lymphoblastic leukemia (B-ALL) is characterized by the presence of the Philadelphia chromosome arising from the t(9;22)(q34;q11.2) translocation (1). The fusion gene constitutively encodes BCR-ABL1 tyrosine kinase, which activates its downstream signaling molecules/pathways (2). The accentuation of these pathways leads to the arrest of B-cell differentiation at an immature stage (progenitor or precursor), followed by uncontrolled proliferation and invasion (3). The use of tyrosine kinase inhibitors (TKIs) is the most effective method for suppressing BCR-ABL1 tyrosine kinase activity (4,5). However, single-agent TKI has not produced sustained responses in BCR-ABL1$^+$ B-ALL, as this specific subtype of B-ALL is likely to develop significant involvement of the CNS, which acts as a 'sanctuary' site for leukemic cells to escape anticancer treatments (6-8). Therefore, understanding the molecular mechanisms of BCR-ABL1$^+$ B-ALL associated with CNS metastasis is a critical step to improve therapeutics.

Previous studies have reported that leukemia follows a blood-vessel track to enter the nervous system, indicating that lymphocytes and leukemic cells may share similar mechanisms of dissemination into tissues (9,10). These cells leave the blood circulation and enter extramedullary tissues by extravasation (9). Following selectin-mediated rolling, cells adhere to endothelial vascular walls by chemokine- and integrin-mediated adhesion to the endothelium (11). Subsequently, lymphocytes and leukemic cells cross the endothelial barrier via transendothelial migration (12,13). The morphological changes and mechanical force required to cross the endothelial barrier rely on integrins and adhesion molecules expressed on lymphocytes or leukemic cells (7,10). These phenomena imply that BCR-ABL1$^+$ leukemic cells also have the ability to enter and disseminate into the CNS. The BCR-ABL1 retroviral bone marrow transduction/transplantation model and the human xenograft NOD/severe combined immunodeficiency (SCID) mouse model are widely used to investigate the mechanisms

of BCR-ABL1+ B-ALL transformation (14,15). However, the characteristics of BCR-ABL1+ B-ALL with CNS metastasis have not been previously investigated, at least to the best of our knowledge.

In the present study, the experimental procedure of BCR-ABL1 retroviral transduction was employed to establish a murine model of BCR-ABL1+ B-ALL with CNS metastasis. The BCR-ABL1+ leukemic cells have an immature B-cell phenotype, including pro-B and pre-B populations with a high expression of integrin subunit alpha 6 (Itga6) and L-selectin adhesion molecules. BCR-ABL1+ leukemic B cells were observed to predominantly invade the meninges, medulla oblongata, cerebrum, cerebellum and lumbar spinal cord. The present results demonstrate that BCR-ABL1+ B-ALL with CNS metastasis is dependent on the intrinsic infiltration ability of BCR-ABL1+ cells, but is independent on increased vascular permeability and structural damage. The present study provides a suitable murine model for studying BCR-ABL1-dependent leukemogenesis and may aid in the development of novel therapeutic strategies for B-ALL disorders.

Materials and methods

Retroviral construction. Murine stem cell virus (MSCV) vector co-expressing human BCR-ABL1 (p210) and green fluorescence protein (GFP; MSCV-BCR-ABL1-IRES-GFP, MIG-p210) and MSCV vector expressing GFP (MIG) have been previously described (16). K562 cells were cultured at 37˚C with 5% CO_2 in RPMI-1640 (HyClone; Thermo Fisher Scientific, Inc.) medium supplemented with 10% fetal calf serum (Gibco; Thermo Fisher Scientific, Inc.). 293T cells were cultured at 37˚C with 5% CO_2 in DMEM (HyClone; Thermo Fisher Scientific, Inc.) medium supplemented with 10% fetal calf serum. 293T cells were transfected with PKAT2 packaging vector and MIG-p210 or MIG using X-tremeGENE HP DNA Transfection reagent (Roche), respectively. At 48 h following transfection, viral supernatants were collected, filtered and stored at -80˚C. K562 and 293T cells were kindly provided by Professor Yanmin Zhang (Xi'an Jiaotong University Health Science Centre).

Bone marrow transduction/transplantation. As previously described (14,15), experimental C57BL/6 mice (age, 7-10 weeks; weight, ~18 g) were purchased from the Experimental Animal Center of Xi'an Jiaotong University and allowed to acclimatize to the environment under specific pathogen-free conditions. The donors (males) and recipients (females) were of the same mouse strain. All animal experiments were performed according to the guidelines of and were approved by the Institutional Animal Care and Use Committee of Xi'an Jiaotong University. In brief, in order to induce ALL, femurs and tibias collected from the donor mice were placed in cold PBS, clipped of the end of the bone, and bone marrow cells were flushed out with PBS. Cells were spun down at 200 x g for 10 min at 4˚C and the supernatant was removed. Bone marrow cells from 2 donor C57BL/6 mice without 5-fluorouracil treatment were subjected to a single round of co-sedimentation with MIG-p210 retroviral supernatants supplemented with 5% WEHI-3B-conditioned medium, 10 ng/ml interleukin (IL)-7 (PeproTech, Inc.) and 20 μg/ml polybrene (Beijing Solarbio Science and Technology Co., Ltd.). The cells were collected 2 h later, washed once in HBSS (Beijing Solarbio Science and Technology Co., Ltd.) and transplanted into lethally irradiated (2x460 cGy) syngeneic 6 female recipient mice ($1x10^6$ cells each) or subjected to culture in RPMI-1640 medium (HyClone, Thermo Fisher Scientific, Inc.) supplemented with 10% fetal calf serum (Gibco; Thermo Fisher Scientific, Inc.), 200 μmol/l L-glutamine, 50 μmol/l 2-mercaptoethanol (Amersco, Inc., Cleveland, OH, USA) and penicillin/streptomycin (HyClone, Thermo Fisher Scientific, Inc.) for 48 h. For the control group, bone marrow cells from 1 donor C57BL/6 mouse were subjected to co-sedimentation with MIG retroviral supernatants and transplanted into 3 recipient mice (details were the same as mentioned above). A GFP+ cell population of >10% was considered to indicate successful transduction. When the transplanted recipient mice exhibited clinical signs of leukemia, which included weight loss, failure to thrive, limb paralysis and splenomegaly, they were euthanized. For secondary transplantation, $1x10^6$, $1x10^5$ and $1x10^4$ bone marrow cells from primary BCR-ABL1+ ALL mice were transplanted into non-irradiated recipient mice, respectively. The secondary transplant recipients were monitored for clinical signs of leukemia as mentioned above for euthanization.

Flow cytometry. The bone marrow and spleen cells were collected from leukemic mice. Red blood cells (RBC) were lysed with NH_4Cl RBC lysis buffer for 5 min at room temperature. The nucleated cells were then washed with cold PBS and stained with anti-Gr1-APC (1:20 dilution; cat. no. 553129; BD Biosciences), anti-CD3-PE (1:20 dilution; cat. no. 561824; BD Biosciences) and anti-CD19-PerCP-Cy$^{TM5.5}$ (1:20 dilution; cat. no. 551001; BD Biosciences) for cell lineages, and incubated with anti-CD43-PE (1:20 dilution; cat. no. 553271; BD Biosciences) and anti-B220-APC (1:20 dilution; cat. no. 553092; BD Biosciences) antibodies for B-cell development. The cells were incubated with the antibodies for 20 min at 4˚C. Analysis was performed using CytoFLEX flow cytometer and the data were analyzed with CytExpert 2.1 (Beckman Coulter, lnc.).

Histology. Mice were anesthetised with chloral hydrate (500 mg/kg) by intraperitoneal injection and the mice were monitored for the absence of tail, foot and ear reflexes, as well as a reduced respiratory rate, which are all indications of effective anesthesia (17). The mice were firstly perfused with 0.9% saline and then with 4% paraformaldehyde in 0.1 M phosphate buffer (pH 7.4). The brain and spinal cord tissues were harvested and post-fixed in 4% paraformaldehyde for 4-6 h at 4˚C. The tissues were then dehydrated in 30% sucrose. All the tissues were embedded in Tek Optimal Cutting Temperature compound (Sakura Finetek Japan Co., Ltd.), sectioned with a semiconductor freezing microtome and stained with hematoxylin and eosin (H&E). For H&E staining (cat. no. G1005; Wuhan Servicebio Co., Ltd.) the slides were washed in PBS and stained with Harris's hematoxylin (10%) for 3-8 min and eosin (70%) for 1-3 min at room temperature. Subsequently, the sections were dehydrated through an increasing concentration of ethanol and xylene. Images of H&E staining were

captured using a Zeiss Axio Scope. A1 microscope (Carl Zeiss Microscopy GmbH).

Wright-Giemsa staining. A 10 μl aliquot of peripheral blood or bone marrow cell flushed out with PBS was spread on a slide to produce a smear and dried at room temperature for 30 min. The smear was fixed with methanol for 15 min and dried at room temperature. The smear was stained with Wright-Giemsa Stain (Heart Biological Technology Co., Ltd) for 8 min at room temperature and was then rinsed with water until the edges turned a pinkish-red color. After air-drying, the smear was inspected under a Zeiss Axio Scope. A1 microscope (Carl Zeiss Microscopy GmbH).

Analysis of CNS metastasis of leukemia by intravascular labeling. Individual BCR-ABL1$^+$ B-ALL mice were intravenously injected with 3 mg anti-CD19-PerCP-Cy$^{TM5.5}$, at 4 min prior to CO_2 euthanasia (flow rate of CO_2 used for the euthanasia of the mice was displaced 20% of the chamber volume per min). Blood was then harvested by cardiocentesis, and mice were subsequently perfused with saline to eliminate residual blood in vessels within tissues (18). The cerebrum, cerebellum, medulla oblongata, meninges, thoracic spinal cord and lumbar spinal cord were dissected and mechanically processed to obtain a single-cell suspension. The samples were examined for GFP and CD19 expression by flow cytometry. BCR-ABL1$^+$ B-ALL cells in the brain tissues were identified as GFP$^+$CD19$^-$ cells, since the anti-CD19 antibody had been removed by saline in the experimental procedure and the B-ALL cells remaining in the vasculature were GFP$^+$CD19$^+$.

Western blot analysis. Cell pellet was collected and lysed in RIPA buffer [50 mM Tris-HCl (pH 8.0), 0.15 M NaCl, 1% Triton X-100, 0.5% NaDoc, 0.1% sodium dodecyl sulphide (SDS), 1 mM ethylenediamine tetraacetic acid (EDTA), 1 mM ethylene glycol tetraacetic acid (EGTA), 1 μM phenylmethane sulphonyl fluoride (PMSF) (Amersco, Inc.) and 1 μg/ml Pepstatin A (Sigma Chemical Co.) protease inhibitors]. Cell lysates were centrifuged for 15 min at 17,000 g at 4˚C and the protein supernatant was collected. Protein concentration was determined via bicinchoninic acid protein assay using a quantification kit (cat. no. BCA02; Beijing Dingguo Changsheng Biotechnology Co., Ltd.). Proteins (40 μg) were run on a 7.5% (w/v) Tris-HCl sodium dodecyl sulphate-poly-acrylamide gel electrophoresis (SDS-PAGE) for electrophoresis, transferred to polyvinylidene difluoride (PVDF) membranes (Millipore Corp, Billerica, MA, USA) and blotted, and then probed with c-ABL antibody (1:1,000 dilution; cat. no. 2862; Cell Signaling Technology, Inc.) overnight at 4˚C. GAPDH (1:25,000 dilution; cat. no. ab9485; Abcam Plc.) was incubated overnight at 4˚C and used as a loading control. The signal was further detected using the secondary antibody of goat anti-rabbit IgG conjugated with horseradish peroxidase (1:5,000 dilution; cat. no. 35560; Thermo Fisher Scientific, Inc.) at room temperature for 1 h. The band signal was visualized by Immobilon™ Western Chemiluminescent HRP substrate (Millipore Corp.).

Reverse transcription-quantitative PCR (RT-qPCR). Total RNA was extracted from the cells using TRIzol reagent (Invitrogen; Thermo Fisher Scientific, lnc.). Complementary DNA (cDNA) was then generated using a PrimeScript™ RT reagent kit (Takara Biotechnology Co., Ltd.) according to the manufacturer's protocol. qPCR was performed with FAST SYBR®-Green Master Mix (Applied Biosystems) using an Mx3000P (Agilent Technologies, Inc.) under following conditions: Initial denaturation at 95˚C for 30 sec; amplified for 40 cycles of 15 sec at 95˚C, 30 sec at 60˚C and 30 sec at 72˚C; dissociation for 1 cycle of 1 min at 95˚C, 30 sec at 55˚C and 30 sec at 95˚C. The relative mRNA levels of genes were calculated using the following equation: $2^{-\Delta\Delta Cq}=2^{-(Cq \text{ target gene-Cq GAPDH) target sample-(Cq target gene-Cq GAPDH) control sample}}$ (19). The following the forward and reverse primers were used: Itga6 5'-GATCCC GGGAGCCTCTTC-3' and 5'-GATGTCACAGCTGTACA GGC-3'; L-selectin, 5'-CTTACTGGGGCTCGAGGAAC-3' and 5'-TCTCTCTTGTTTTGTATGGCGAC-3'; GAPDH, 5'-CGTCCCGTAGACAAAATGGT-3' and 5'-AGGTCAATG AAGGGGTCGTT-3'.

Statistical analysis. Statistical analysis was performed using SPSS 20.0 (IBM Corp.) and GraphPad Prism 6.0 (GraphPad Software). For continuous variables, descriptive results were presented as the means ± standard error of the mean (SEM). Levene's test was used for equality of variances. The independent-samples t-test, one-way analyses of variance (ANOVA) with post-hoc Fisher's LSD test and log-rank Mantel-Cox analysis were performed for 2-group comparisons, multiple groups comparisons and survival comparisons, respectively. Kaplan-Meier survival curves wereused to describe the changes of survival rate with time. $P<0.05$ was considered to indicate a statistically significant difference.

Results

Establishment of a murine model of BCR-ABL1$^+$ ALL with extramedullary hematopoietic site infiltration. To generate a murine model of BCR-ABL1$^+$ ALL with metastasis, $1x10^6$ bone marrow cells harvested from donor mice were subjected to co-sedimentation with a retrovirus co-expressing BCR-ABL1 and GFP, and then transplanted into syngeneic lethally irradiated recipient mice. Of the primary recipients, 100% exhibited symptoms of clinical leukemia with hind limb paralysis to various degrees or other observable CNS symptoms, weight loss, respiratory or other types of distress, or extreme lethargy. The leukemic mice were euthanized from 40 to 83 days following transplantation (Fig. 1A-C). As a result of cachexia, the maximum percentage of body weight loss observed in the leukemic mice was 15.23% (Fig. 1C). The peripheral blood contained lymphoblastic cells with 32.00% GFP$^+$ cells (Fig. 1D). The bone marrow cells appeared to be of a lymphoblastic phenotype with 43.49% GFP$^+$ cells (Fig. 1E). The leukemic mice developed splenomegaly with 54.21% GFP$^+$ cells (Fig. 1F) and lymphadenopathy with 86.83% GFP$^+$ cells (Fig. 1G). These results indicate that the transplanted mice developed classical ALL. Furthermore, BCR-ABL1$^+$ leukemic cells were observed to metastasize to the subcutaneous tissues, lung and liver with varying amounts of GFP$^+$ cells (Fig. 2A-C and Table I). Of note, the degree of infiltration into the lymph nodes and subcutaneous tissues was significantly higher compared with that into other tissues in

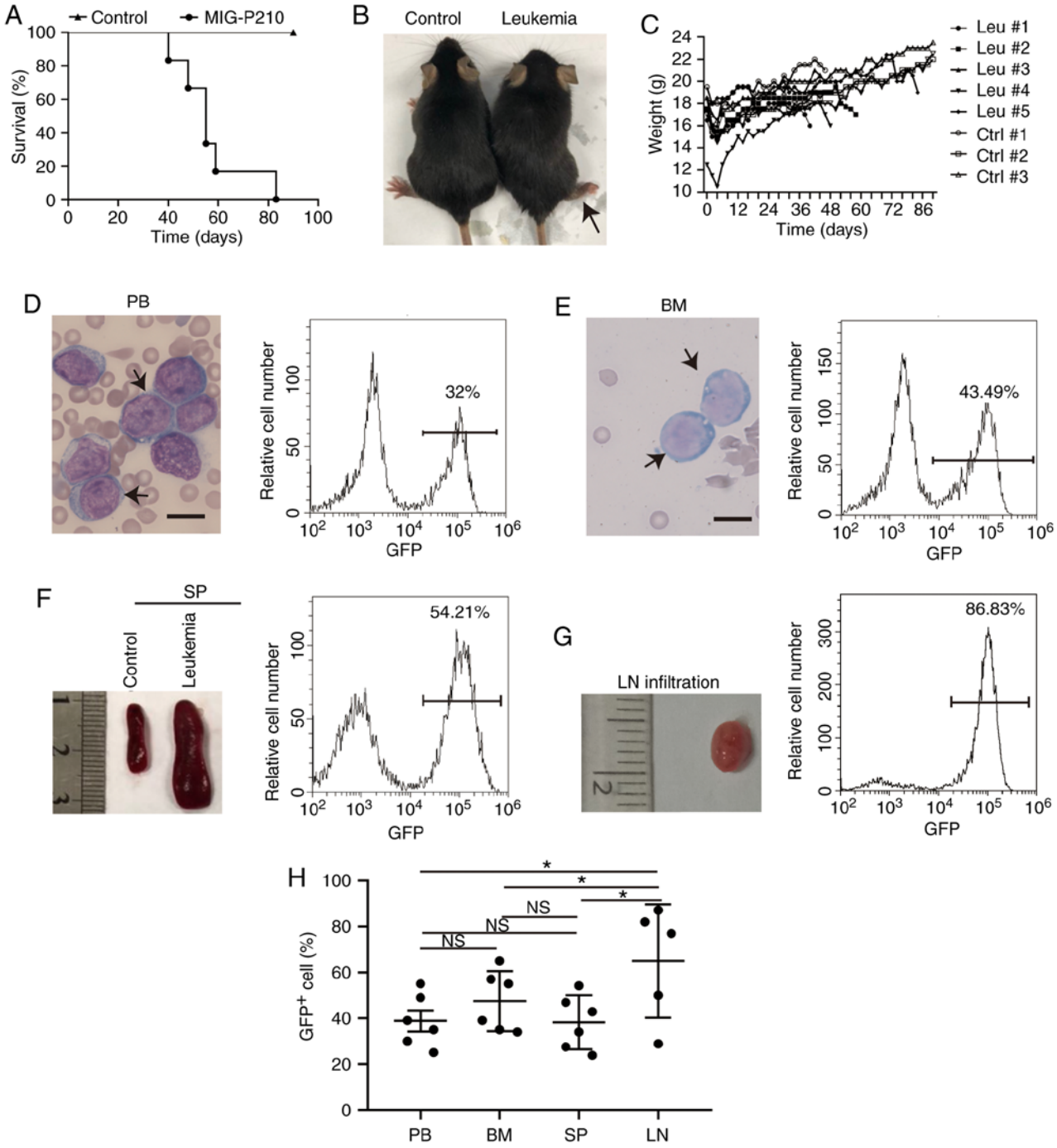

Figure 1. Establishment of mouse BCR-ABL1+ ALL models. (A) Kaplan-Meier survival curves of syngeneic lethally irradiated recipient mice transplanted with donor bone marrow cells transduced by the MIG-p210 (n=6) or MIG (Control, n=3) retroviral supernatants, respectively. (B) Representative leukemic mouse showing hind leg paralysis, as indicated by the black arrow. (C) Monitoring of body weights of leukemic and control mice until they were euthanized. Leukemic mice (Leu, n=6) and control mice (Ctrl, n=3). (D) Peripheral blood (PB) lymphoblastic cells were stained by Wright-Giemsa indicated with the black arrows and the PB GFP+ cell percentage was detected by flow cytometry in a leukemia mouse. Scale bar, 10 μm. (E) Bone marrow (BM) lymphoblastic cells were stained by Wright-Giemsa (indicated by black arrows) and the BM GFP+ cell percentage was examined by flow cytometry in one leukemic mouse. Scale bar, 10 μm. (F) Gross appearance of the spleen (SP) and the percentage of GFP+ cells of SP in one leukemic mouse. (G) Gross appearance of the lymph node (LN) and the percentage of GFP+ cells of LN in one leukemic mouse. (H) Scatter plot showing the percentages of GFP+ cells in BCR-ABL1+ ALL mice. PB (n=6), BM (n=6), SP (n=6) and LN (n=5). Data indicate the means of independent mouse data with the error bars representing the SEM. *P<0.05; NS, not significant, P>0.05 (PB vs. BM, P=0.350; PB vs. SP, P=0.947; PB vs. LN, P=0.012; BM vs. SP, P=0.318; BM vs. LN, P=0.049; SP vs. LN, P=0.011).

the BCR-ABL1+ ALL mice (Figs. 1H and 2D). BCR-ABL1 expression were detected in the bone marrow, spleen and subcutaneous tissues (Fig. 2E). Taken together, these results demonstrate that the mouse model of BCR-ABL1+ ALL with infiltration into non-hematopoietic tissues was successfully established by using the BCR-ABL1 retroviral transduction system.

BCR-ABL1+ leukemic cells have a B-lymphoid lineage-specific immunophenotype. To precisely define the BCR-ABL1+

Table I. Summary of metastasis in primary transplantation.

Mouse ID	Hind limb paralysis	Spleen metastasis	Subcutaneous metastasis	Lymph node metastasis	Lungmetastasis	Liver metastasis
1#	+	+	+	-	+	+
2#	+	+	-	-	ND	ND
3#	+	+	-	-	ND	ND
4#	+	+	+	+	+	+
5#	+	+	-	+	ND	ND
6#	+	+	+	-	+	+

+, metastasis occurred; -, metastasis did not occur; ND, metastasis was not detected.

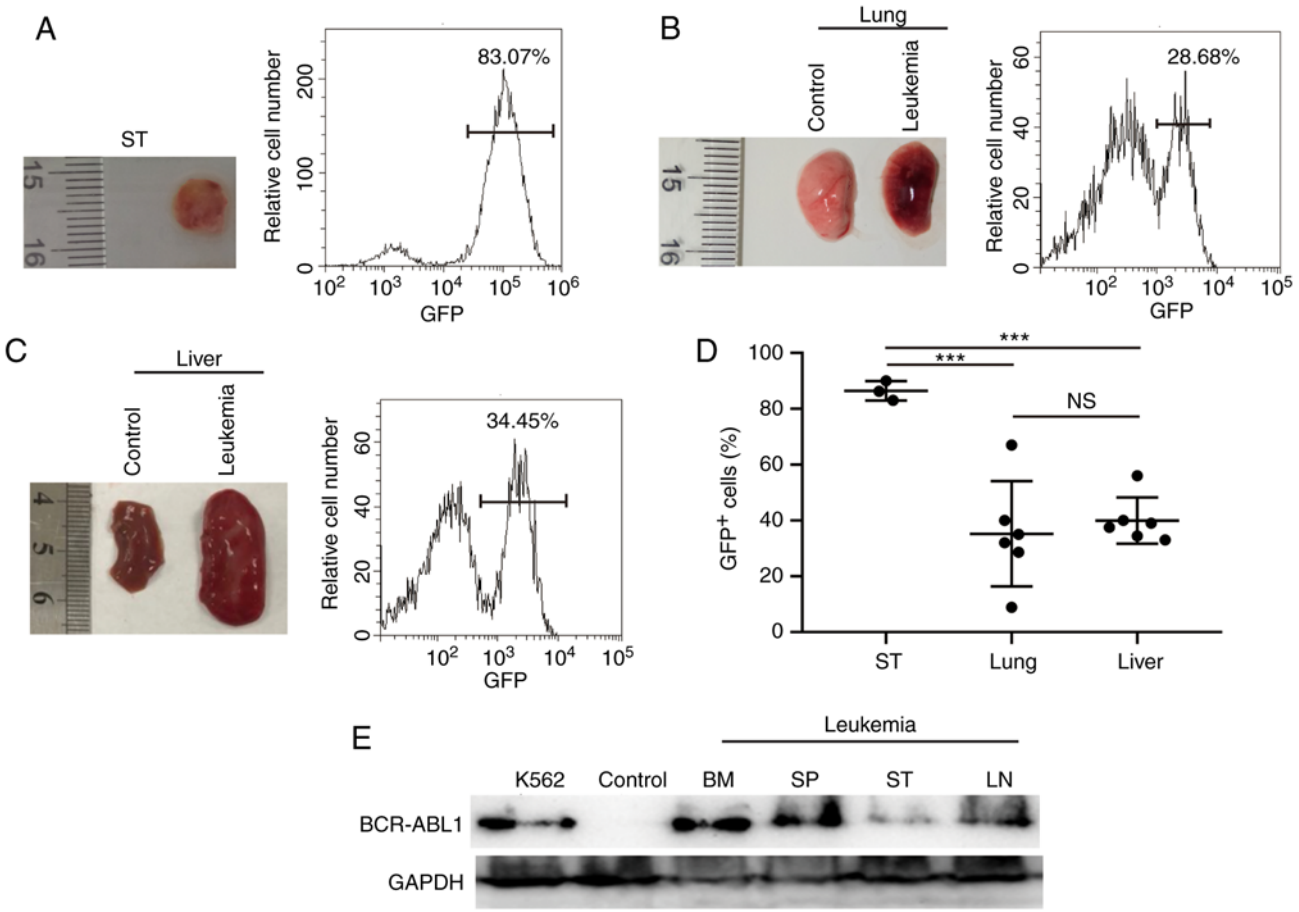

Figure 2. The various extramedullary hematopoietic infiltrations in BCR-ABL1$^+$ ALL mice. (A) Gross appearance of the subcutaneous tumor (ST) and the percentage of GFP$^+$ cells of ST in one leukemic mouse. (B) Gross appearance of the lung and the percentage of GFP$^+$ cells of the lung in one leukemic mouse. (C) Gross appearance of the liver and the percentage of GFP$^+$ cells of the liver in one leukemic mouse. (D) Scatter plot showing the percentages of GFP$^+$ cells in *BCR-ABL1*$^+$ ALL mice. ST (n=3), lung (n=6) and liver (n=6). Data indicate the means of independent mouse data with the error bars representing the SEM. ***P<0.001; NS, not significant, P>0.05 (ST vs. lung, P<0.001; ST vs. liver, P<0.001; lung vs. liver, P=0.550). (E) BCR-ABL1 and endogenous c-abl expression were measured by immunoblots. Ku80 protein was used as a loading control. BCR-ABL1$^+$ K562 cell line and bone marrow cells transfected with retrovival MIG (Control) were served as positive control and negative control for BCR-ABL1 protein expression, respectively.

lymphoblastic cells with respect to their phenotype and lineage origin, it was examined whether BCR-ABL1$^+$ leukemic cells were lineage-specific. The bone marrow or spleen cells from leukemic mice were incubated with antibodies against Gr1 for myeloid cells, CD3 for T-lymphoid cells and CD19 for B-lymphoid cells, respectively, and analyzed by flow cytometry. The results indicated that GFP$^+$ cells derived from individual leukemic mice expressed the B lymphoid-specific marker CD19, but not CD3 or Gr1 (Fig. 3A and B, and Fig. S1A and B), suggesting that the BCR-ABL1$^+$ leukemic cells were of the B-cell lineage. To evaluate the B-cell development stage of the leukemic GFP$^+$CD19$^+$ population, the CD43- and B220-expressing cells among GFP$^+$ cells were gated. The results indicated that GFP$^+$ cells contained a variable

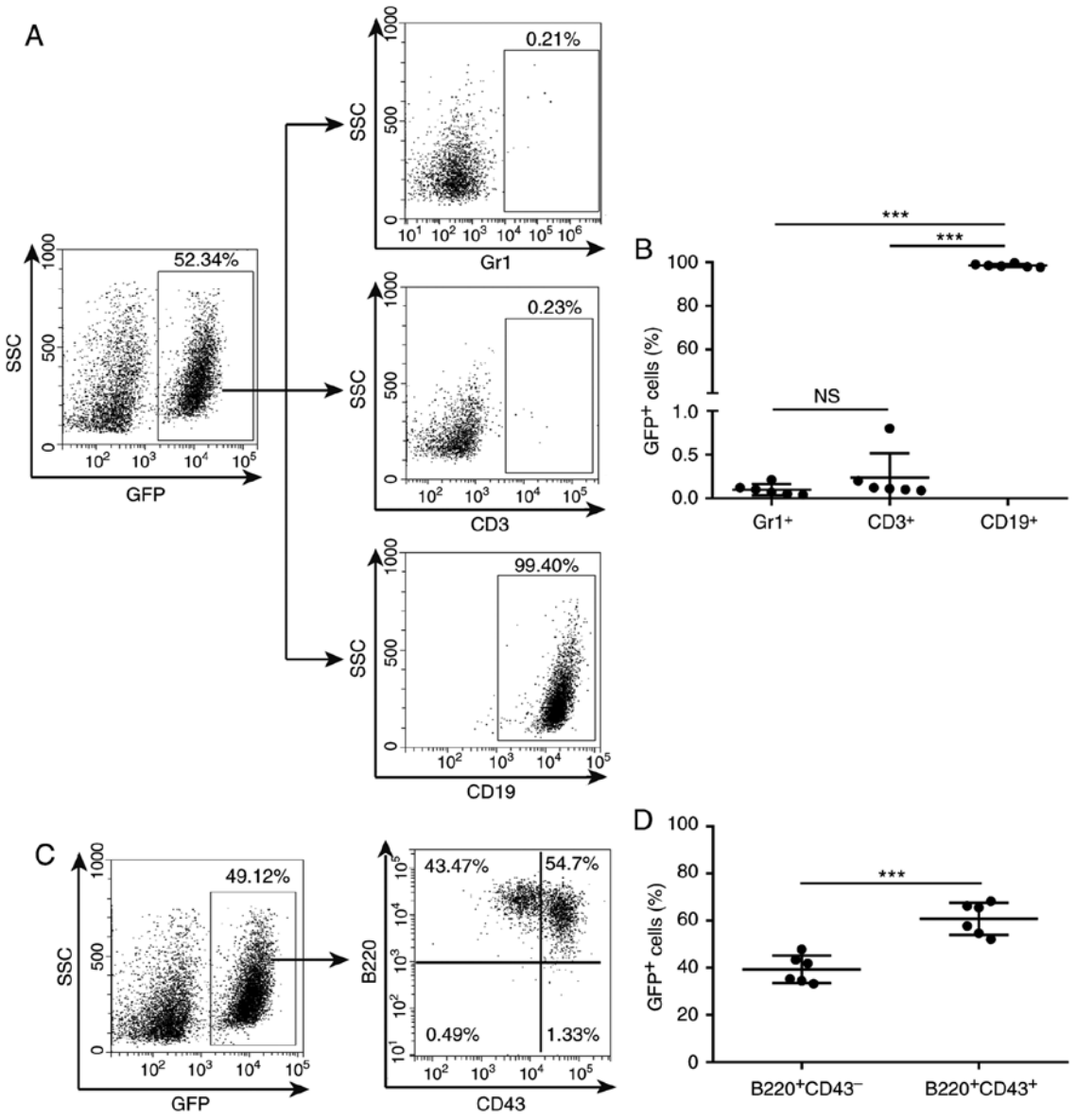

Figure 3. BCR-ABL1+ leukemic cells are impaired at pro-B/pre-B stages of B cell development. (A) Representative flow cytometric analysis of bone marrow (BM) cells from a BCR-ABL1+ ALL mouse. GFP+ cells expressed B cell lineage antigen CD19 (bottom panel), and lacked expression of myeloid lineage antigen Gr1 (top panel) and T cell lineage antigen CD3 (middle panel). (B) Scatter plot showing the percentages of Gr1, CD3 and CD19 antigens on GFP+ cells in BCR-ABL1+ ALL mice (n=6). ***P<0.001. (C) Representative flow cytometric analysis of BM cells from a BCR-ABL1+ ALL mouse. GFP+ cells expressed CD43 and B220 antigens. Data indicate the means of independent mouse data with the error bars representing the SEM. NS, not significant, P>0.05 (Gr1+ vs. CD19+, P<0.001; CD3+ vs. CD19+,P<0.001; Gr1+ vs. CD3+, P=0.595). (D) Scatter plot showing the percentages of CD43+B220+ and CD43-B220+ populations on GFP+ cells in BCR-ABL1+ ALL mice (n=6). Data indicate the means of independent mouse data with the error bars representing the SEM. ***P<0.001 (CD43+B220+ vs. CD43-B220+, P<0.001).

proportion of CD43 and B220 populations (Fig. 3C and D, and Fig. S1C and D), suggesting that the BCR-ABL1+ leukemic cells remained fixed at the pro-B to pre-B stage of B-cell development. The results demonstrated that almost all BCR-ABL1+ leukemic cells exhibited a pro-B/pre-B cell immunophenotype and that the BCR-ABL1+ leukaemia murine model generated in the present study may be classified as BCR-ABL1+ B-ALL.

BCR-ABL1+ B-ALL leukemic cells invade the CNS. Since the BCR-ABL1+ B-ALL mice exhibited severe CNS symptoms, the lumbar spinal cord and cerebellar tissues were first dissected for H&E staining in the BCR-ABL1+ B-ALL mice and healthy control mice, respectively. The histological sections revealed a significant number of leukemic cells in the lumbar spinal cord and meninges of the BCR-ABL1+ B-ALL mice compared to the healthy controls (Fig. 4), suggesting that the BCR-ABL1+ cells had already invaded into the CNS when the leukemic mice developed clinical symptoms of limb paralysis.

Subsequently, to identify the exact proportions of leukemic infiltration in the nervous system, an intravascular staining approach was pursued. First, the anti-CD19 antibody was injected into the vasculature of BCR-ABL1+ B-ALL mice and the blood was then harvested immediately. The leukemic mouse was perfused with saline to remove residual blood cells and anti-CD19 antibody after euthanasia. The single-cell suspension was collected from the blood, brain parenchyma,

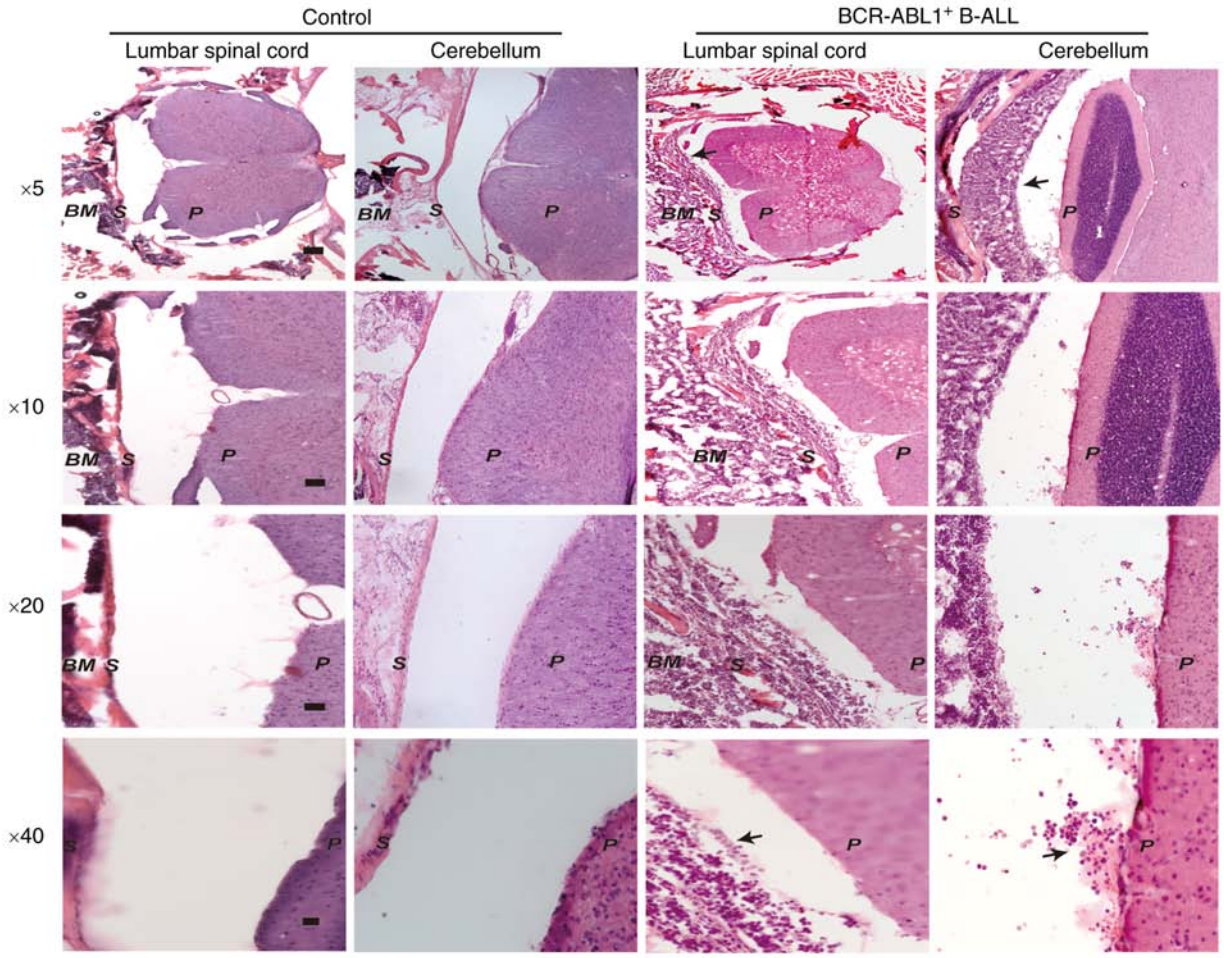

Figure 4. BCR-ABL1$^+$ leukemic cells infiltrate into lumbar spinal cord and cerebellum. Representative H&E staining of lumbar spinal cord and cerebellum sections from a BCR-ABL1$^+$ B-ALL mouse (the two panels on the right) and a healthy control mouse (the two panels on the left) at x5 (scale bars, 200 μm), x10 (scale bars, 100 μm), x20 (scale bars, 50 μm) and x40 (scale bars, 20 μm) magnification. BM, bone marrow. S, skull. P, brain parenchyma. Leukemic infiltration is indicated by black arrows.

meninges and spinal cord, and further analyzed for GFP and CD19 expression. The BCR-ABL1$^+$ B-ALL leukemic cells in the vasculature revealed a GFP$^+$CD19$^+$ population, as the cells were stained by anti-CD19 antibody (Fig. 5A). The leukemic cells that had infiltrated into the CNS had no opportunity to be stained by anti-CD19 antibody and were only GFP$^+$, and their proportion varied between the meninges (72.70%), lumbar spinal cord (8.84%), medulla oblongata (4.25%), cerebrum (4.14%) and cerebellum (3.25%; Fig. 5B and C), which was in agreement with the observation from H&E staining that massive leukemic cell infiltration had occurred in the meninges. In addition, no infiltration in the thoracic spinal cord was observed, indicating that the leukemic cells in the lumbar spinal cord probably did not originate from the spreading of CNS residual leukemia by extension along spinal nerves. These results suggest that the BCR-ABL1$^+$ B-ALL cells have the ability to enter and disseminate into the CNS.

BCR-ABL1$^+$ B-ALL leukemic cell invasion into the CNS is dependent on their own intrinsic properties. To further confirm whether the BCR-ABL1$^+$ B-ALL with CNS metastasis was driven by the ability of leukemic cells to enter and disseminate into the CNS, experiments were performed using immunocompetent recipient mice injected with $1x10^6$, $1x10^5$ or $1x10^4$ primary BCR-ABL1$^+$ leukemic cells. Irradiation-induced CNS damage was avoided through this injection. It was observed that the secondary recipients developed BCR-ABL1$^+$ leukemia with severe paralysis of their hind limbs within 25 days following transplantation (Fig. 6A and B). The onset of secondary leukemia was shorter in comparison with that of primary leukemia (Fig. 1A). The morphological lymphoblastic cells were enriched in the peripheral blood and bone marrow (Fig. 6C and D). The immunophenotype of GFP$^+$ cells displayed a B-cell lineage with block at pro-B to pre-B stages of B-cell development (Fig. 6E). Of note, the percentage of GFP$^+$ cells in the CNS of secondary BCR-ABL1$^+$ B-ALL was significantly increased when compared to that in primary B-ALL (Fig. 6F). These results re-emphasize that BCR-ABL1$^+$ leukemogenic cells have their own intrinsic properties to induce B-ALL with a high incidence of CNS infiltration.

It was hypothesized that the molecules associated with adhesion are deregulated in BCR-ABL1$^+$ B-ALL mice (20). The expression of cell adhesion molecule Itga6 and L-selectin was detected in splenic GFP$^+$CD19$^+$ cells sorted from primary and secondary BCR-ABL1$^+$ B-ALL mice. The splenic CD19$^+$ cells derived from healthy mice were used as controls. The results indicated that the transcripts of Itga6 and L-selectin were

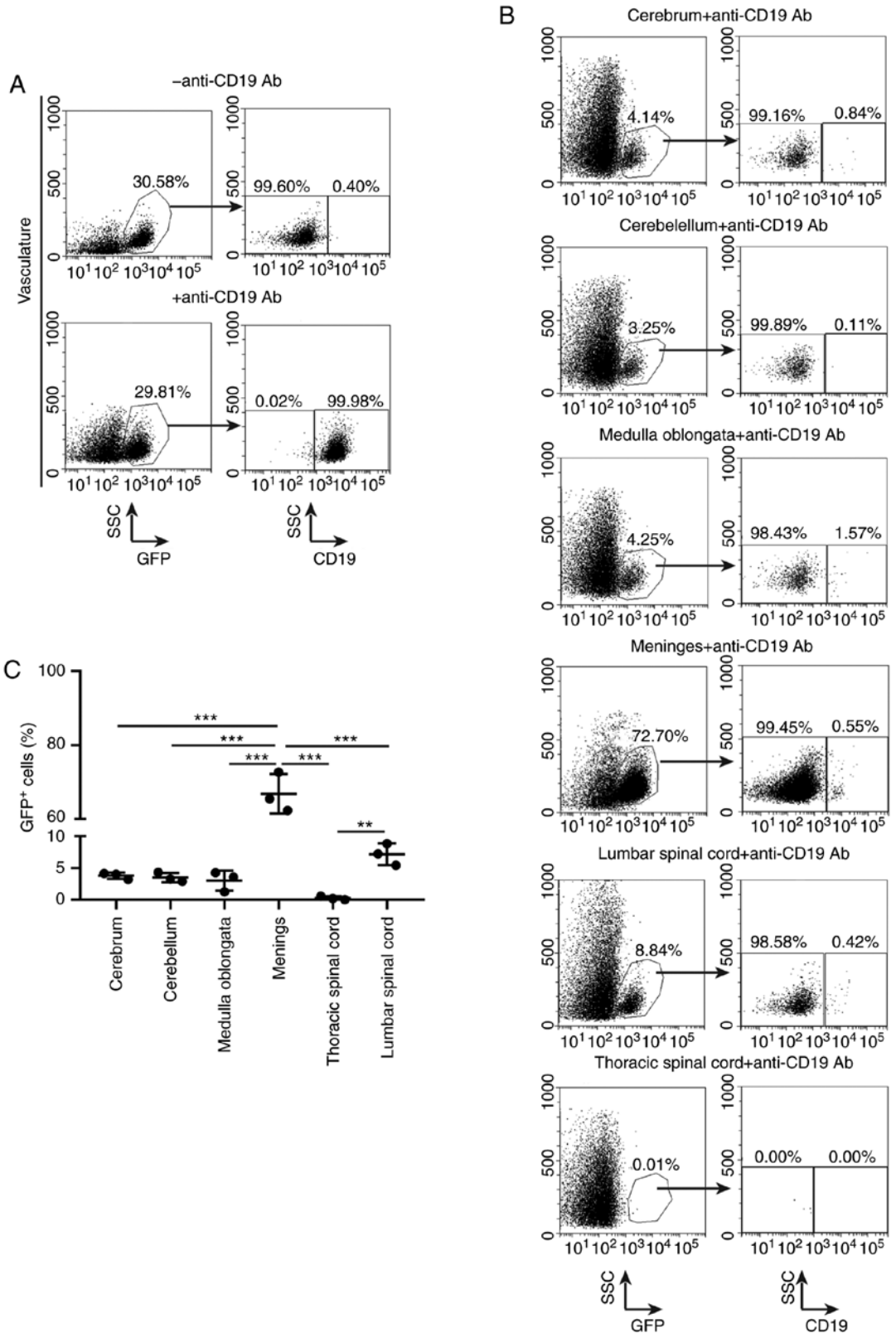

Figure 5. Evaluation of BCR-ABL1+ B-ALL leukemic cell accumulation in various central nervous system (CNS) tissues. Representative flow cytometric analysis of leukemic cells metastasis into the nervous system. (A) The BCR-ABL1+ B-ALL mouse was intravenously injected with CD19-PerCP-Cy$^{TM5.5}$ antibodies then quickly euthanized. Living cells were gated by forward- and side-scatter (data not shown), and then gated on side-scatter and GFP (left panels). GFP+ cells arrested in the vasculature were labelled by CD19+ gate (right panels). (B) Living cells from various CNS tissues were gated by forward- and side-scatter (data not shown), followed by gating on side-scatter and GFP (left). GFP+ cells were gated on CD19 to distinguish CD19+ and CD19- population depending on whether brain parenchyma GFP+ cells had either already metastasized before injection with CD19-PerCP-Cy$^{TM5.5}$ antibodies or had been contaminated by vessel leukemic cells during dissection, respectively (right panels). (C) Scatter plot showing the percentages of GFP+ cells in CNS derived from BCR-ABL1+ ALL mice. cerebrum (n=3), cerebellum (n=3), medulla oblongata (n=3), meninges (n=3), lumbar spinal cord (n=3), thoracic spinal cord (n=3). Data indicate the means of independent mouse data with the error bars representing the SEM. **P<0.01 and ***P<0.001 (cerebrum vs. meninges, P<0.001; cerebellum vs. meninges, P<0.001; medulla oblongata vs. meninges, P<0.001; thoracic spinal cord vs. meninges, P<0.001; lumbar spinal cord vs. meninges, P<0.001; lumbar spinal cord vs. thoracic spinal cord, P=0.004; P-values between other groups were no significance).

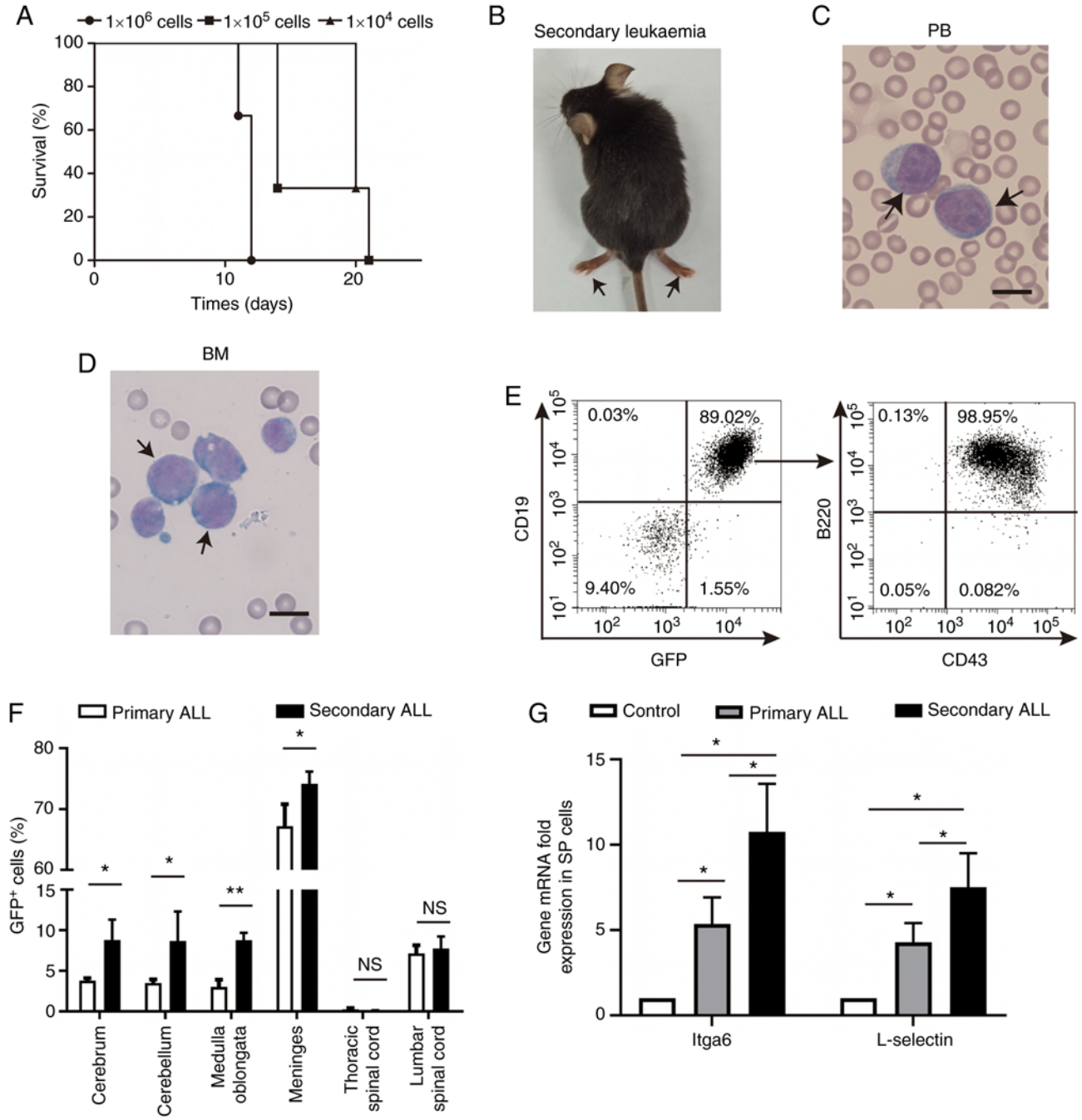

Figure 6. The characterization of BCR-ABL1$^+$ B-ALL from secondary transplantation. (A) Kaplan-Meier survival curves of syngeneic nonirradiated mice transplanted with 1x10^6, 1x10^5 and 1x10^4 splenic cells from primary BCR-ABL1$^+$ B-ALL mice, respectively. Each group contains 3 mice. (B) Representative transplanted mouse developed leukemia with paralysis of hindquarters indicated as the black arrows. (C and D) Lymphoblastic cells from PB and BM were stained by Wright-Giemsa and indicated as the black arrows, respectively. Scale bar, 10 μm. (E) The majority of GFP$^+$ cells blocked at pro-B stage, indicated as CD43$^+$B220$^+$ population. (F) The percentages of BCR-ABL1$^+$ B leukemic cells metastasized into different tissues of CNS labeled as GFP$^+$CD19$^-$ in primary B-ALL mice (n=3) and secondary B-ALL mice (n=3) by using intravascular staining. Data indicate the means of independent mice with the error bars representing the SEM. *P<0.05 and **P<0.01; ns, no significant difference. (G) Transcripts of Itga6 and L-selectin genes were detected in splenic GFP$^+$CD19$^+$ cells from primary B-ALL mice (n=3) and secondary B-ALL mice (n=3), respectively. Transcripts of Itga6 and L-selectin genes from splenic CD19$^+$ cells of healthy mice (n=3) were used as controls. Gene mRNA fold expression values have been normalized to the GAPDH as described in Methods. Data indicate the means of independent mouse with the error bars representing the SEM. *P<0.05.

upregulated in primary and secondary BCR-ABL1$^+$ B-ALL compared with those in healthy control mice, respectively (Fig. 6G and Fig. S2). Furthermore, the expression levels of Itga6 and L-selectin were also significantly increased in the secondary BCR-ABL1$^+$ B-ALL mice compared with those in the primary ones. These results may imply that in BCR-ABL1$^+$ B-ALL mice, the invasion of BCR-ABL1$^+$ leukemic cells into the CNS probably depends on abnormal gene expression associated with metastasis.

Discussion

BCR-ABL1$^+$ B-ALL has a poor prognosis and is associated with refractoriness and CNS damage (21-24). Current disease

models fail to precisely resemble BCR-ABL1+ B-ALL with CNS infiltration, posing a limitation for *in vivo* studies aiming at elucidating the pathogenesis of the disease and the associated mechanisms. In the present study, a mouse model of BCR-ABL1+ B-ALL with CNS metastasis was established. The majority of the BCR-ABL1+ cell population were immature B cells with a pro-B/pre-B phenotype. BCR-ABL1+ B-ALL cells were found in CNS tissues at various proportions, with a specific accumulation in the meninges. BCR-ABL1+ B-ALL cells have the ability to propagate, maintain their phenotypes, and upregulate Itga6 and L-selectin expression, which, together, are associated with migration or metastasis. With these characteristics, the newly established model of BCR-ABL1+ B-ALL with CNS metastasis may provide further insight into the pathogenesis of BCR-ABL-mediated leukemogenesis.

Previous studies have been reported that approximately 30-50% of patients with *BCR-ABL1*+ ALL harbor the p210 fusion protein, with the remaining 50-70% being characterized by the p190 fusion protein (25). The *BCR-ABL1* fusion oncogene exists in two principal forms (p190 and p210) that arise from distinct breakpoints in the *BCR* gene on chromosome 22, resulting in translocation of *BCR* exon 1 or exons 1-12/13, respectively, to the c-*ABL1* gene on chromosome 9. p210 and p190 contain the same portion of the c-ABL1 tyrosine kinase and acquire uncontrolled tyrosine kinase activity, both of which constantly turn on the downstream signaling molecules/pathways, and promoting proliferation of leukemia cells (16). Previous studies have reported that chronic myeloid leukemia (CML) can be reproduced in mice by the retroviral transduction of p190 or p210 into hematopoietic stem cell (HSC)-enriched bone marrow (BM) cells in the presence of myeloid cytokines, followed by transplantation into irradiated recipients (14,26), which is a myeloproliferative disorder characterized by the increased proliferation of granulocytic cells without the loss of their capability to differentiate (27-30).

In the present study, this approach was utilized by donor bone marrow cells pre-stimulated with the lymphoid cytokine IL-7, which provides critical signals for B-cell proliferation and survival (31,32). As a result, the mouse p210+ B-ALL mouse model was not only successfully generated, but it was also observed that prominent infiltration in non-hematopoietic tissues with clinical severe paralysis of CNS was achieved. The present results indicated that the majority of the leukemic cells may be characterized as immature pro-B ($CD43^+B220^+$) and pre-B ($CD43^-B220^+$) populations (33-36). In addition to this observation, rare GFP+ cells, either from the bone marrow or spleen, lacked expression of lineage-specific antigens (data not shown), implying that the BCR-ABL1+ B-ALL cells contain leukemic stem and progenitor cells and propagate leukemia to the next generation. It was also demonstrated that the transplantation of primary BCR-ABL1+ B-ALL cells is capable of generating secondary B-ALL in non-irradiated mice. This murine model resembles human BCR-ABL1+ B-ALL and may be used to study the prognosis of human B-ALL.

The model established in the present study has an attractive feature of enabling leukemic cells to expand into various types of non-hematopoietic tissue, including the CNS, subcutaneous tissue, lung and liver. H&E staining and intravascular staining technology were applied to precisely assess the exact portions of leukemic cells dissemination into CNS. The results suggest that leukemic cells are predominantly deposited in the meninges, medulla oblongata, cerebrum, lumbar spinal cord and cerebellum, which is consistent with the results of previous studies (37-39). A previous study detected small vessels transiting between the bone marrow and subarachnoid space in leukemic mice, and it was indicated that numerous openings in the vertebral cortical bone were filled with ALL cells, which appeared to be in transit between the bone marrow involved and the subarachnoid space (13,40). Therefore, BCR-ABL1+ leukemic cells may directly metastasize into the lumbar spinal cord, but not into the thoracic spinal cord.

Laminin is localized in the extracellular matrix of meninges, the choroid plexus and peripheral nerve sheaths in the nervous system (41,42). Metastasis to the CNS has been indicated to be mediated through the interaction of molecules associated with cell motility and adhesion (43). This information supports the present result that highly expressed Itga6 and L-selectin may allow BCR-ABL1+ B-ALL leukemic cells to interact with laminin located in the ECM of meninges. This specific interaction hijacks and recruits leukemic cells into the meninges, but fails to enter the brain parenchyma (7,12,42,43). These results support the phenomenon that a large number of leukemic cells accumulate in the meninges.

In conclusion, in the present study, a murine model of BCR-ABL1+ B-ALL with CNS metastasis was generated. The infiltrated BCR-ABL1+ immature B cells have the ability to metastasize in various proportions into the CNS, with significant accumulation in the meninges, which may be associated with the upregulation of numerous adhesion molecules, including Itga6 and L-selectin. These results encourage further studies to address whether TKIs combined with the targeting of proteins associated with cell migration and adhesion may offer a therapeutic approach for the CNS metastasis/relapse of BCR-ABL1+ B-ALL.

Acknowledgements

The authors would like to thank Professor Shaoguang Li from the Division of Hematology/Oncology, University of Massachusetts Medical School, for providing the MIG-p210 construct. The authors would also like to thank Mr. Huixun Ren (Xi'an Jiaotong University Health Science Centre) for assisting the with mouse colony maintenance and Mr. Xiaofei Wang (Xi'an Jiaotong University Health Science Centre) for providing expert technical assistance with cell sorting.

Funding

This study was supported by grants (no. 31170821, no. 31370874 and no. 81670157) from the National Natural Scientific Foundation of China and by a grant (no. 2016JZ030) from the Natural Scientific Foundation of Shaanxi.

Availability of data and materials

All data generated or analyzed during this study are included in this published article and its supplementary information files.

Authors' contributions

XY, HZ and MZ performed the experiments and participated in designing some experiments. MY, PZ and YW participated in the experiment of viral supernatants and article revision. YW, ZL and WOO performed the flow cytometry experiments, and CLi, CLiu, YJ and YM performed some of the *in vivo* experiments. XY and YJ wrote the manuscript. All authors have read and approved the manuscript and agree to be accountable for all aspects of the research in ensuring that the accuracy or integrity of any part of the work are appropriately investigated and resolved.

Ethics approval and consent to participate

All animal procedures were approved by the Institutional Animal Care and Use Committee of Xi'an Jiaotong University.

Patient consent for publication

Not applicable.

Competing interests

The authors declare that they have no competing interests.

References

1. Bernt KM and Hunger SP: Current concepts in pediatric Philadelphia chromosome-positive acute lymphoblastic leukemia. Front Oncol 4: 54, 2014.
2. Quintás-Cardama A and Cortes J: Molecular biology of bcr-abl1-positive chronic myeloid leukemia. Blood 113: 1619-1630, 2009.
3. Schjerven H, Ayongaba EF, Aghajanirefah A, McLaughlin J, Cheng D, Geng H, Boyd JR, Eggesbø LM, Lindeman I, Heath JL, *et al*: Genetic analysis of Ikaros target genes and tumor suppressor function in BCR-ABL1^{+} pre-B ALL. J Exp Med 214: 793-814, 2017.
4. Pfeifer H, Wassmann B, Hofmann WK, Komor M, Scheuring U, Brück P, Binckebanck A, Schleyer E, Gökbuget N, Wolff T, *et al*: Risk and prognosis of central nervous system leukemia in patients with Philadelphia chromosome-positive acute leukemias treated with imatinib mesylate. Clin Cancer Res 9: 4674-4681, 2003.
5. Mullighan CG: The molecular genetic makeup of acute lymphoblastic leukemia. Hematology Am Soc Hematol Educ Program 2012: 389-396, 2012.
6. Hamdi A, Mawad R, Bassett R, di SA, Ferro R, Afrough A, Ram R, Dabaja B, Rondon G, Champlin R, *et al*: Central nervous system relapse in adults with acute lymphoblastic leukemia after allogeneic hematopoietic stem cell transplantation. Biol Blood Marrow Transplant 20: 1767-1771, 2014.
7. Trendowski M: The inherent metastasis of leukaemia and its exploitation by sonodynamic therapy. Crit Rev Oncol Hematol 94: 149-163, 2015.
8. Jabbour E, Thomas D, Cortes J, Kantarjian HM and O'Brien S: Central nervous system prophylaxis in adults with acute lymphoblastic leukemia: Current and emerging therapies. Cancer 116: 2290-2300, 2010.
9. Arbonés ML, Ord DC, Ley K, Ratech H, Maynard-Curry C, Otten G, Capon DJ and Tedder TF: Lymphocyte homing and leukocyte rolling and migration are impaired in L-selectin-deficient mice. Immunity 1: 247-260, 1994.
10. Campbell JJ, Hedrick J, Zlotnik A, Siani MA, Thompson DA and Butcher EC: Chemokines and the arrest of lymphocytes rolling under flow conditions. Science 279: 381-384, 1998.
11. Ley K, Laudanna C, Cybulsky MI and Nourshargh S: Getting to the site of inflammation: The leukocyte adhesion cascade updated. Nat Rev Immunol 7: 678-689, 2007.
12. Nourshargh S, Hordijk PL and Sixt M: Breaching multiple barriers: Leukocyte motility through venular walls and the interstitium. Nat Rev Mol Cell Biol 11: 366-378, 2010.
13. Yao H, Price TT, Cantelli G, Ngo B, Warner MJ, Olivere L, Ridge SM, Jablonski EM, Therrien J, Tannheimer S, *et al*: Leukaemia hijacks a neural mechanism to invade the central nervous system. Nature 560: 55-60, 2018.
14. Peng C and Li S: CML mouse model in translational research. Methods Mol Biol 602: 253-266, 2010.
15. Roumiantsev S, de Aos IE, Varticovski L, Ilaria RL and Van Etten RA: The src homology 2 domain of Bcr/Abl is required for efficient induction of chronic myeloid leukemia-like disease in mice but not for lymphoid leukemogenesis or activation of phosphatidylinositol 3-kinase. Blood 97: 4-13, 2001.
16. Li S, Ilaria RL, Million RP Jr, Daley GQ and Van Etten RA: The P190, P210, and P230 forms of the BCR/ABL oncogene induce a similar chronic myeloid leukemia-like syndrome in mice but have different lymphoid leukemogenic activity. J Exp Med 189: 1399-1412, 1999.
17. Maheras KJ and Gow A: Increased anesthesia time using 2,2,2-tribromoethanol-chloral hydrate with low impact on mouse psychoacoustics. J Neurosci Method 219: 61-69, 2013.
18. Anderson KG, Mayer-Barber K, Sung H, Beura L, James BR, Taylor JJ, Qunaj L, Griffith TS, Vezys V, Barber DL and Masopust D: Intravascular staining for discrimination of vascular and tissue leukocytes. Nat Protoc 9: 209-222, 2014.
19. Livak KJ and Schmittgen TD: Analysis of relative gene expression data using real-time quantitative PCR and the 2(-Delta Delta C(T)) method. Methods 25: 402-408, 2001.
20. Krause DS, Katherine L, Lewis JB, Andrian UH and Van Etten RA: Selectins and their ligands are required for homing and engraftment of BCR-ABL1^{+} leukemic stem cells in the bone marrow niche. Blood 123: 1361-1371, 2014.
21. Levinsen M, Taskinen M, Abrahamsson J, Forestier E, Frandsen TL, Harila-Saari A, Heyman M, Jonsson OG, Lähteenmäki PM, Lausen B, *et al*: Clinical features and early treatment response of central nervous system involvement in childhood acute lymphoblastic leukemia. Pediatr Blood Cancer 61: 1416-1421, 2014.
22. Camicia R, Winkler HC and Hassa PO: Novel drug targets for personalized precision medicine in relapsed/refractory diffuse large B-cell lymphoma: A comprehensive review. Mol Cancer 14: 207, 2015.
23. Krause S, Pfeiffer C, Strube S, Alsadeq A, Fedders H, Vokuhl C, Loges S, Waizenegger J, Ben-Batalla I, Cario G, *et al*: Mer tyrosine kinase promotes the survival of t(1;19)-positive acute lymphoblastic leukemia (ALL) in the central nervous system (CNS). Blood 125: 820-830, 2015.
24. Buchner M, Swaminathan S, Chen Z and Müschen M: Mechanisms of pre-B-cell receptor checkpoint control and its oncogenic subversion in acute lymphoblastic leukemia. Immunol Rev 263: 192-209, 2015.
25. Score J, Calasanz MJ, Ottman O, Pane F, Yeh RF, Sobrinho-Simões MA, Kreil S, Ward D, Hidalgo-Curtis C, Melo JV, *et al*: Analysis of genomic breakpoints in p190 and p210 BCR-ABL indicate distinct mechanisms of formation. Leukemia 24: 1742-1750, 2010.
26. Gu S, Sayad A, Chan G, Yang W, Lu Z, Virtanen C, Van Etten RA and Neel BG: SHP2 is required for BCR-ABL1-induced hematologic neoplasia. Leukemia 32: 203-213, 2018.
27. Dong Y, Liu F, Wu C, Li S, Zhao X, Zhang P, Jiao J, Yu X, Ji Y and Zhang M: Illegitimate RAG-mediated recombination events are involved in IKZF1 Δ3-6 deletion in BCR-ABL1 lymphoblastic leukaemia. Clin Exp Immunol 185: 320-331, 2016.
28. Morotti A, Panuzzo C, Crivellaro S, Pergolizzi B, Familiari U, Berger AH, Saglio G and Pandolfi PP: BCR-ABL disrupts PTEN nuclear-cytoplasmic shuttling through phosphorylation-dependent activation of HAUSP. Leukemia 28: 1326-1333, 2014.
29. Dash AB, Williams IR, Kutok JL, Tomasson MH, Anastasiadou E, Lindahl K, Li S, Van Etten RA, Borrow J, Housman D, *et al*: A murine model of CML blast crisis induced by cooperation between BCR/ABL and NUP98/HOXA9. Proc Natl Acad Sci USA 99: 7622-7627, 2002.
30. Zhang H, Peng C, Hu Y, Li H, Sheng Z, Chen Y, Sullivan C, Cerny J, Hutchinson L, Higgins A, *et al*: The Blk pathway functions as a tumor suppressor in chronic myeloid leukemia stem cells. Nat Genet 44: 861-871, 2012.
31. Vegh P, Winckler J and Melchers F: Long-term 'in vitro' proliferating mouse hematopoietic progenitor cell lines. Immunol Lett 130: 32-35, 2010.

32. Holl TM, Haynes BF and Kelsoe G: Stromal cell independent B cell development in vitro: Generation and recovery of autoreactive clones. J Immunol Methods 354: 53-67, 2010.
33. Ji Y, Resch W, Corbett E, Yamane A, Casellas R and Schatz DG: The in vivo pattern of binding of RAG1 and RAG2 to antigen receptor loci. Cell 141: 419-431, 2010.
34. Dong Y, Wu C, Zhao X, Zhang P, Zhang H, Zheng M, Li S, Jiao J, Yu X, Lv Z and Ji Y: Epigenetic modifications of the VH region after DJH recombination in Pro-B cells. Immunology 152: 218-231, 2017.
35. Hardy RR and Hayakawa K: B cell development pathways. Annu Rev Immunol 19: 595-621, 2001.
36. Wu C, Dong Y, Zhao X, Zhang P, Zheng M, Zhang H, Li S, Jin Y, Ma Y, Ren H and Ji Y: RAG2 involves the Igκ locus demethylation during B cell development. Mol Immunol 88: 125-134, 2017.
37. Pippard MJ, Callender ST and Sheldon PW: Infiltration of central nervous system in adult acute myeloid leukaemia. Br Med J 1: 227-229, 1979.
38. Prieto C, López-Millán B, Roca-Ho H, Stam RW, Romero-Moya D, Rodríguez-Baena FJ, Sanjuan-Pla A, Ayllón V, Ramírez M, Bardini M, *et al*: NG2 antigen is involved in leukemia invasiveness and central nervous system infiltration in MLL-rearranged infant B-ALL. Leukemia 32: 633-644, 2018.
39. Roddie P, Collie D and Johnson P: Myelomatous involvement of the dura mater: A rare complication of multiple myeloma. J Clin Pathol 53: 398-399, 2000.
40. Cheung LC, Tickner J, Hughes AM, Skut P, Howlett M, Foley B, Oommen J, Wells JE, He B, Singh S, *et al*: New therapeutic opportunities from dissecting the pre-B leukemia bone marrow microenvironment. Leukemia 32: 2326-2338, 2018.
41. Colognato H, ffrench-Constant C and Feltri ML: Human diseases reveal novel roles for neural laminins. Trends Neurosci 28: 480-486, 2005.
42. Wang L, Dong Z, Zhang Y and Miao J: The roles of integrin β4 in vascular endothelial cells. J Cell Physiol 227: 474-478, 2012.
43. Salomão DR, Pulido JS, Johnston PB, Canal-Fontcuberta I and Feldman AL: Vitreoretinal presentation of secondary large B-cell lymphoma in patients with systemic lymphoma. JAMA Ophthalmol 131: 1151-1158, 2013.